Design, Construction, Calibration and Testing of a Wind Tunnel Force Balance

André Filipe Rocha Oliveira
andrerochaoliveira@tecnico.ulisboa.pt

Instituto Superior Técnico, Universidade de Lisboa, Portugal

September 2020

Abstract

Experimental activities are essential in the aerospace industry, with wind tunnels being the most used devices in the validation of concepts and design. Therefore, this work aims to endow the Aerospace Engineering Laboratory at Instituto Superior Técnico with an aerodynamic balance capable of measuring forces and moments. The balance follows an existing *Stewart* platform configuration design, here readjusted to the current requirements. The design and validation of mechanical performance were initially done computationally using *SolidWorks*$^{®}$, then some experimental tests were performed for verification. In addition to the construction, the instrumentation of the balance was necessary to compute forces and moments, as well as additional quantities for the tests, such as speed, temperature and attitude. To this end, strain gauges and several sensors were studied and implemented. The balance user interface was done in *LabVIEW*^{TM}. To make the balance as accurate as possible, a static calibration was performed to relate the application of well-known loads on the balance with the response of the strain gauges. This way, it was possible to obtain a matrix with calibration coefficients for all aerodynamic components using the collected data and the least squares method with a second-order polynomial. Finally, an experimental test was performed with a model of the rear wing of a racing car to confirm the optimisation in C_L/C_D when using endplates with a curved profile instead of a flat profile. The influence of velocity in the rear wing performance was also analysed and a comparison with CFD was carried out.

Keywords: Wind tunnel, Aerodynamic force balance, Mechanical design, Sensors and instrumentation, Calibration, Experimental tests

1. Introduction

The wind tunnels are, without any doubt, the most used facilities for experimental tests. A scale model of an aircraft or a component, such as a wing, is used in wind tunnel tests in aerospace. In these facilities, the scale model is subjected to an air flow. From this interaction, forces, moments, pressures, flow visualisations and others can be obtained as a result. This data is processed in terms of dynamics and stability of the model.

Just as the wind tunnels are the most common tests facilities, the aerodynamic force balance is the most well-known test instrument. Since forces and moments are common quantities to measure in a wind tunnel, it is almost inevitable to find an aerodynamic force balance in wind tunnels facilities. The scale models are trustworthy reproductions of common size aircrafts or space vehicles. The use of a small-scale model instead of the real object is mostly justified by the easiness of obtaining results for more handleable pieces.

The wind tunnel installed in the Aerospace Engineering Laboratory at Instituto Superior Tecnico (Técnico) currently lacks readily available instrumentation. As such, the motivation of this work is to provide capability of measuring aerodynamic forces by developing an aerodynamic force balance capable of running out experimental tests. The force balance needs to be able to obtain the three components of the aerodynamic forces (vertical, horizontal and lateral) and the aerodynamics moments (pitch, roll and yaw). In addition, other quantities will be provided by other support sensors, such as speed, temperature, humidity and model attitude. This way, the Técnico wind tunnel will be upgraded to supply a higher variety of experimental tests to the student and research activities.

To achieve the desirable force balance, all the process stages need to be overcome, ranging from design to testing, with some intermediate steps. After introduced a suitable design to the mechanical requirements, manufacture and assembly is mandatory, as well, the development and coupling of instrumentation. As the force balance must pro-

vide trustfully data, calibration is introduced and demonstration is provided.

2. Background

2.1. Wind Tunnel

In a wind tunnel, air and aircraft change the roles once assumed in flight. Instead of having the aircraft moving in the air, the aicraft is fixed and the air forced to move around it. An adequately scaled model, corresponding to an aerodynamically equivalent aircraft, can be used in wind tunnels. The conditions of operation in wind tunnel are set to reproduce the same results as those obtained in real aircraft operation.

There are many different variations of wind tunnels. They can be divided into two main groups: the open air circuit and the closed air circuit. The open circuit wind tunnel does not have re-circulation of air, instead the air enters from an open area and exits to another open area. Closed circuit wind tunnels have re-circulation of air, with little or no air exchange with the exterior [1].

The major tests proceed in wind tunnel are divided into: pressure, force and visualisation.

2.2. Force Balance

A force balance is a device that allows the measurement of forces and moments, commonly used in wind tunnels testing. Two different configurations of force balance are widely used: internal and external. External force balances are placed in the test section and the model is mounted over some part of the balance. Internal force balances are placed inside the model [2].

The *Stewart* platform is a mechanism well-known in external force balance configurations. The mechanism are constituted by two platforms which are connected by bars. The fixation between the bars and the platform is made by a spherical joints. The six non collinear bars create a system with six degrees of freedom, three translations and three rotations.

The *Stewart* platform features different configurations but the most common are the so-called 3-3, 3-6 and 6-6 formats. Each configuration name regards the number of platform vertex and connections between them. However, a new type of configuration is normally introduced to adapt the stability of the 3-3 configuration and solve the problem of creating double spherical joints [3]. This configuration is a type of 6-6 configuration based in a 3-3 configuration, as seen in Figure 1 .
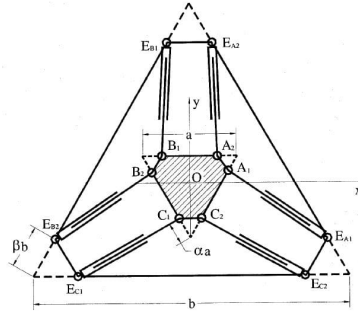

Figure 1: 6-6 *Stewart* platform based on the 3-3 platform [3].

3. Mechanical Design

3.1. Requirements

Two loads cases sets were considered for sizing the force balance, one for the half wing and the other for the aircraft model, see Table 1

Test Case	F_X [N]	F_Y [N]	F_Z [N]	M_X [N.m]	M_Y [N.m]	M_Z [N.m]
Half-wing	-109	966	0	241	27	46
Aircraft	-75	-24	-390	1	-15	1

Table 1: Load cases for the force balance.

The design of the force balance depends on two design specifications: the limit loads and the acceptable displacements. The acceptable displacements are those that still maintain the apparatus in its set desired position

The critical mechanical parts of the force balance are the sensing bars, whose extension will be measured and the strain (ϵ) computed. To make the deformation controllable, the bars must work under the elastic deformation regime, defined by the *Hooke's law*, $\sigma = E\epsilon$, where E is the *Young's Modulus* and σ is the stress [4]. Therefore the limit acceptable force to tension is provided by the material *Yield Stress* and $Force = \sigma A$, where A is the cross-section area of the bar.

In case of compression, the bar cannot suffer the *buckling* phenomenon. The critical force for which the buckling occurs (P_{Cr}) is computed by the *Euler's critical load* formula,

$$P_{Cr} = \frac{C_{fix}\pi^2 E I}{l^2} \qquad (1)$$

where the C_{fix} is a constant that depends on the conditions of the fixation of the column, I is the minimum area moment of inertia and the l is the length of the column. For a fixed column with rotation in both ends, the C_{fix} corresponds to 1 [4].

The displacements are a consequence of the forces and moments applied on the force balance. These displacements are in the form of rotations and translations of some components. A large displacement of this component would introduce a variation of the initial setting parameters that are desired to keep constant: this parameters are the angle of attack and the side-slip angle of the model.

Therefore, the displacements are measured at the top part of the force balance in terms of the angles variation over the Y-axis (angle of attack) and the Z-axis (side-slip angle). The limit applied is that both of incremental angles cannot be greater than $0.5°$.

3.2. Computational Structural Analysis

The design of all parts and all computational analyses of the force balance is made in *Solid-Works*®. The CAD was adapted for the current requirements and specifications from a precious work. The simulations have as base a simplified CAD to reduce computational effort. The structural analyses are made with a finite elements method, and the mesh used is based in parabolic tetrahedral solid elements Mesh convergence studies were made, for both the aircraft model force balance and for the half wing model force balance, using the total strain energy. The number of elements set for the subsequent analyses are 202 046 for the aircraft case and 245 445 for the half wing case.

From the first computational analysis, the *Yield Stress* ($241E+06$ N/m^2) and the critical buckling force (2260 N) were respected for each sensing bar, but these parameters were deemed not important at this stage since the strain values were close to one micrometre ($1E-06$), being this the lower advisable measurement limit of the available strain sensor. A higher strain value was desirable for a better use of the reading scale and to respect the recommended values.

3.3. New Parts Design

The redesign of the sensing bars had as principal objective an improvement of the strain measurement, which could be done by manipulating its cross-section area. The sensing bar sizing was made by taking into account three criteria: the *Yield Stress*, the buckling critical force and a measurement sensitivity of 1N. To verify if the sensing bar was able to measure increments of 1N, an experimental test was carried out.

The first sizing attempt was made with a large cross reduction, by reducing the previous thickness from 1.5mm to 0.45mm (7mm of outer diameter and 6.1mm of inner diameter). Despite this first attempt satisfied the first two criteria for the aircraft model force balance and the strain response to 1N increments, Figure 4, a premature assembly of six of these bars and the fixed and moving platforms introduced damage,such as bending and rupture, to the bars, Figure 2.

The new sensing bar design selected was a combination of two cross-sections diameters with requiring more manufacture but fit the requirements. This bar had the initial selected outer and inner diameter, 10mm and 7mm, but there was a middle

Figure 2: Damage occurred during the assembly of the first sensing bars.

section of 100mm in which the wall thickness had been reduced to 1mm (outer diameter of 9mm and inner diameter of 7mm), Figure 3.

Figure 3: Manufacture of the new sensing bar

All the criteria of selection was satisfied, the *Yield Force* and *buckling* force is higher than the maximum expected forces for both study cases and the response to 1N increments was detected to every weights, see Figure 4. To determine the minimum length so that the stress is uniform, a computational tensile test of the new sensing bar was performed with a 1500N force. The stress is uniform after $\approx$ 10mm of the reduction wedge.
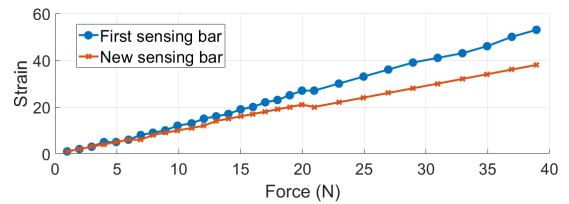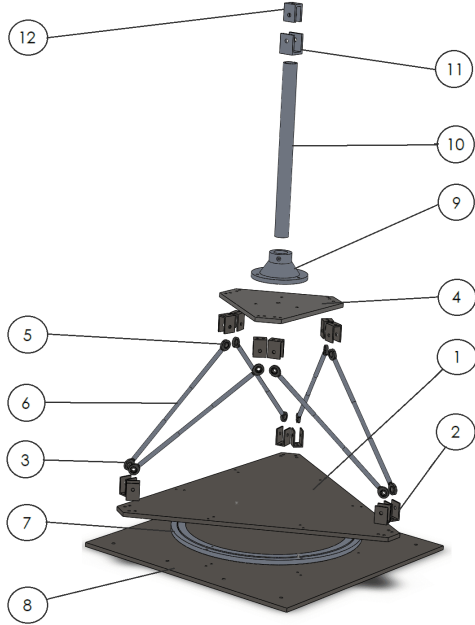

Figure 4: Strain response for experimental load set.

Other additional changes were introduced in the design. The top platform thickness was increased from 5mm to 10mm and the material is now Al 6082-T6 instead of composite. The wall thickness of the strut was reduced, by changing the inner diameter from 20mm to 25mm. It was also adopted a new design for the flange.

3.4. New Force Balance Assembly

The new assembly, Figure 5, introduces significant improvements in respect of the strain, and the necessity of a better use of the reading scale is satisfied without compromising the critical displacements. The increments of angle of attack and side-

slip angle are 0.22° and 0.36° in the worst cases. The maximum computed force, 1666.8N, is 28% of the *Yield Force* and the maximum compressive force, -1502.44N, is 67% of the maximum P_{cr} for the new sensing bars, respecting *Yield Stress* and *Buckling* criteria.
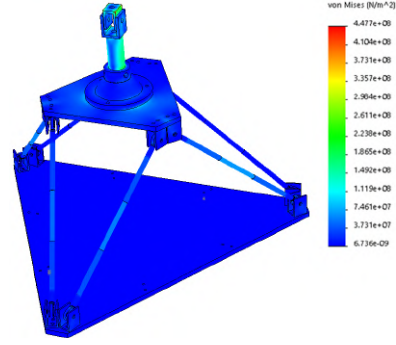

Figure 6: Stress plot of one force balance model.

in electrical resistance is produced when a strain variation is applied to the gauge [2]. The strain gauge selected was the *1-LY13-6/350* by HBM. This strain gauge integrates a specific group of strain gauges to be attached on aluminium, with a nominal resistance is 350Ω and a strain gauge factor of $2.11 \pm 1.0\%$.

The number of strain gauges and the orientation depends on the *Wheatstone* bridge used, quarter-bridge, half-bridge and full-bridge. The half-bridge uses two sensors perpendicular to each other, allowing to measure the axial deformation with one sensor and the other sensor to shear strain, compensate this way the *Poisson* effect [5]. This type of *Wheatstone* bridge were selected, due to the compensation of *Poisson* effect and given the forces on the sensing bars are purely axial. The half-bridge uses less sensors than a full-bridge, this carries less associated costs and simplify the placement of the strain gauges. The reduced bar cross-area will introduce more complexity in the placement pursuant to the number of strain gauges used. The misalignment of the strain gauges can affect the accuracy of the measurements. The half-bridge do not have the same temperature compensation as the full-bridge. However, the temperature is controlled inside the facilities and additional components can be introduced to minimise the temperature effect.

To create a half-bridge, two strain gauges were required in each sensing bar. To ensure uniform strain, the strain gauges were placed in the middle of the reduced middle section of the bar and with a clearance of 10mm between both gauges to prevented interference issues. The placement of the strain gauge followed a specific steps, the final instrumented sensing bar is presented in Figure 7.

4.2. Sensing Bar Strain Gauge System Calibration

The expected strain response from the bar gauge system is linear with the application of force, since the working regime is elastic making the stress-strain linear. However, the creation of the physical system is associated with some deviations from the

Item number	Part name	Quantity	Material
1	FixedPlatform	1	Steel 1.0037
2	Coupler	12	Alloy Steel
3	RodEndBearing_R	6	Steel 1.0503 Brass
4	NewMovingPlatform	1	Al 6082-T6
5	RodEndBearin_L	6	Steel 1.0503 Brass
6	NewSensingBar	6	Al 6063-T6
7	RotatingCollar	1	Al 2024-T4 Al 6063-T6
8	Table	1	Steel 1.0037
9	NewFlange	1	Al 7075-T6
10	NewStrut	1	Al 6063-T6
11	alphaAdjustment_1	1	Al2024-T4
12	alphaAdjustment_2	1	Al 2024-T4

Figure 5: Exploded view of the new force balance model assembled.

The mechanical setup was concluded with a stress analysis of the complete force balance model and confirmation that the *Yield Stress* is respected in all of its components as demonstrated in Figure 6.

The maximum stress is $2.44\mathrm{E}+07\mathrm{N/m}^2$ for the aircraft model and $2.48\mathrm{E}+08\mathrm{N/m}^2$ for half wing model, well below the *Yield Stress* of $3.25\mathrm{E}+08\mathrm{N/m}^2$.

4. Instrumentation
4.1. Strain Gauge

A strain gauge is an electromechanical device where the electrical resistance can be related with the strain in the component directly, a change
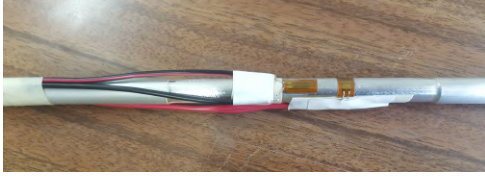
4

Figure 7: Strain gauges placed on the sensing bar.

theoretical analyses. The placement of the strain gauges, the material imperfections and geometrical deviations are examples of the causes of the difference between experimental and theoretical results. A calibration of the strain response to a well-known loading force removes any intermediate strain matching process and introduce more accuracy to the force balance.

The calibration procedure consisted in loading each sensing bar with a load sequence and taking the strain response. Each weight was verified using a high-resolution scale. The loading experiment used the *NI 9237* board to compute the strain from the bridges. The experimental data collection was continuous to not introduce variations in the initial setting configurations. The strain values for each increment was averaged in the most uniform part.

As expected, the response of the strain was not exactly linear but close for the six sensing bars. Three types of adjustment regressions were made for each bar, 1st order, 3rd order and 5th order, parabolic equations do not fit this case, Figure 8.The parameter of interest is the R^2 of each regression, and from the obtained values, the regression that best fits the compromise between a R^2 close to 1 and the computational effort is cubic regression.
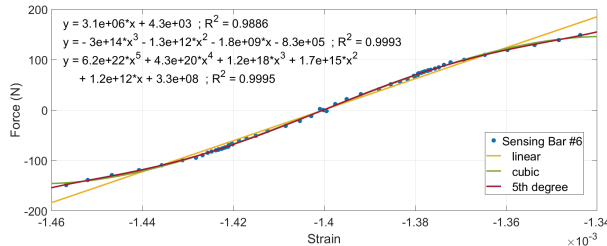

Figure 8: Force for average strain response for sensing bar number # 6.

4.3. Speed, Temperature and Attitude Sensor

To obtain the speed of the air flow in the test section, a differential pressure sensor was required to related the static pressure and dynamic pressure by the *Bernoulli's* equation

$$p_0 - p_s = \frac{1}{2}\rho V^2 \Leftrightarrow V = \sqrt{\frac{2}{\rho}(p_o - p_s)} \quad (2)$$

The pressure sensor *MPXV7002DP* is an analogical sensor able to compute the difference between the dual pressure intakes. With a dual intake Pitot tube and a processing system, the system to obtain the flow speed was complete.

For the force balance case, the temperature measured will be the air flow temperature inside the chamber so the range of temperature is small and close to the common environment temperatures. The *DHT11* is a temperature and humidity sensor with reduced dimensions with a range of temperatures from 0°C to 50°C, and of humidity from 20% to 90%.

An inertial measurement unit (IMU) combines several inertial sensors, being the most common accelerometers to measure the external force acting on the sensor and gyroscopes to measure the sensor angular velocity. The IMU uses a specific process to obtain position and direction [6]. The digital *MPU-6050* is a typical IMU with three orthogonal mounted accelerometers and three orthogonal mounted gyroscopes. This allows the measurement of the angle of attack and side-slip angle of the model.

4.4. Arduino Solution

Each sensor needs a set of instructions to initialise and compute the quantities through the sensor outputs. This coding for each sensor will be running on the Arduino and is made using the Arduino *IDE*software.

The *MPXV7002DP* provide the difference of the two pressure intakes as output, and is present on the form of voltage. A transfer function provides the conversion of this voltage output to pressure units

$$\Delta P = 1000 \left(\frac{5V_{out}}{V_s} - \frac{5}{2} \right) \quad (3)$$

Applying this tansfer function, analog to digital conversion (ADC) and Equation (2), the final equation to compute the velocity appears

$$v = \sqrt{\frac{10000 \left(\frac{ADC\ Reading}{2^{10}-1} - \frac{1}{2} \right)}{\rho}} \quad (4)$$

where the *ADC Reading* is the reading from the Arduino.

The sensor *DHT11* provides digital output of values in final user reading form. The code follows the most simple structure sequence of the Arduino IDE.

The *MPU 6050* sensor initial position should be a position set by the user. An additional code was created to reset the sensor to a desired initial position. It returns six values with establish the actual sensor position. These offsets are then introduced in a specific part of the *MPU 6050* code. The rest of the code was made to give to the user the variation of *yaw*, *pitch* and *roll* in degrees, measured form the initial position. The angle of attack and side-slip can be set with the variation of *pitch* and

yaw, respectively.

One Arduino had enough input pins and processing power and memory to handle the three sensors. Each sensor requires one power supply and one ground, the outputs pins vary with the sensor. The schematic wire connection to the Arduino is shown in Figure 9.
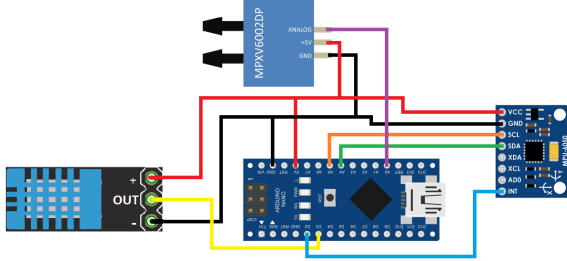

Figure 9: Wire connection scheme of the pressure, temperature and attitude sensor with the Arduino.

The final acquisition code is a merger of the three individual codes which process the three quantities at the same time in loop. The measured temperature is used to compute the air density through the ideal gas law $\left(\rho = \frac{p_s}{R_{specific}T}\right)$.

4.5. Data Acquisition System and User Interface

The *NI 9237* board by *National Instruments*[TM] is a CompactDAQ capable of measuring signals from quarter-bridge, half-bridge and full-bridge. Each board has 4 input channels on the form of *RJ50*, each capable of reading one bridge signal. This DAQ is configured with *LabVIEW*[TM] [7].

The *NI 9237* has a internal system with replace the use of external resistances to complete the bridge, this system is more stable and more practical to use. The connection of an half-bridge to the *NI 9237* board is depicted in Figure 10.
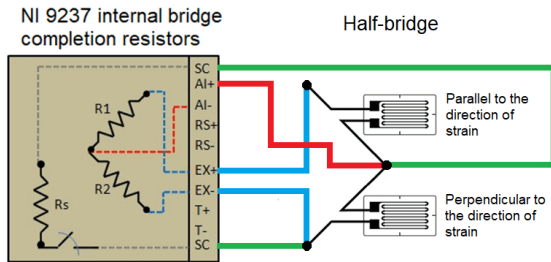

Figure 10: Connection between a half-bridge and a *RJ50* gate on the *NI 9237* board.

The user interface, created with *LabVIEW*[TM], gathers the necessary parameters to provide the aerodynamic forces and moments on the final form. The instantaneous values of forces and moments can be seen on numerical and graphical form, and are also saved to file.

The additional instrumentation process the data through Arduino *IDE*. Therefore, both scripts should run at the same time. The additional instrumentation provides the air flow speed, temperature, humidity, and the model *yaw*, *pitch* and *roll* angles.

5. Manufacture and Assembly

Some of the designed parts corresponded to an off-the-self product to simplify the acquisition, while the rest was manufactured. The manufacture of the force balance parts could be outsourced or made in-house. The selection of manufacture was strongly dependent on the form in which the raw material is provided and the facilities required to machine it. The force balance parts manufactured in-house was the sensing bars, the flange and a support for the pitot tube.

Table 2 presents the materials required to manufacture the components, the purchased components, the purchased instrumentation and the additional parts for assembly. The costs and quantities are shown, as well.

	Product	Quantity	Price (€)
	Table	1	121.52
	Fixed platform	1	117.86
	Coupler	12	210.18
	Alpha adjustment 1	1	69.86
	Alpha adjustment 2	1	69.37
	Rotating collar	1	57.58
	Rod end bearing (INA GAL8-UK)	6	115.79
Mechanical	Rod end bearing (INA GAR8-UK)	6	115.79
	New strut	1	9.84
	Tubo redondo 10x1,5 mm (1m)∗	6	9.84
	Circular block ø130mm (0.08m)∗	1	36.75
	New moving platform	1	97.42
	Angle beam, plate and block ∗	-	8.83
	Rubber supports for table	8	11.32
	Bolts, nuts, rings, insulating tube, clamps	-	18.37
	Subtotal		1070.32
	Strain gauges (1-LY13-6/350)	30	247.95
	Attitude sensor *MPU 6050*	1	6.09
	Temperature sensor *DHT11*	1	3.69
Electrical	Pressure sensor *MPXV7002DP*	1	12.79
	Arduino nano	1	11.00
	DAQ *NI 9237*	2	2790.00
	Cables, connectors, RJ50 plugs, boxes, hoses, USB hub, USB extension cable	-	55.87
	Subtotal		3127.39
	Total		4197.71

∗ Raw material for the manufacture of the force balance component.

Table 2: Force balance costs breakdown.

The coupling of all the parts, both mechanical assembly concerning all structural components and electrical assembly concerning the integration of the instrumentation, is partially shown in Figure 11 for

the bottom part of the force balance with all the required instrumentation. The sensing bars are instrumented with the strain gauge and coated with insulating tube.

Figure 11: Final assembly.

6. Calibration

The six desired aerodynamics quantities (drag, lift, side, rolling, pitching and yawing) cannot be immediately computed due to the lack of relations between these quantities and the sensing bars strain gauges outputs. The calibration solve this final stage by correlating these two quantities.

The aerodynamic components are represented by f_i, being f_1 drag, f_2 lift, f_3 side force, f_4 roll, f_5 pitch and f_6 yaw moment. The input variable of the model will be presented was r_j, with $j = 1, ..., 6$, and corresponding to the sensing bar force converted from voltage output of the strain gauge bridge.

The aerodynamic forces are dependent of the sensing bar forces and also of the calibration coefficients. The number of coefficients and the complexity of the model are dependent with the order of the model [8]. The second-order model expanded and simplified is

$$
\begin{aligned}
f_i = & r_1 c_{i,1} + r_2 c_{i,2} + r_3 c_{i,3} + r_4 c_{i,4} + r_5 c_{i,5} + r_6 c_{i,6} \\
& + r_1^2 c_{i,7} + r_1 r_2 c_{i,8} + r_1 r_3 c_{i,9} + r_1 r_4 c_{i,10} + r_1 r_5 c_{i,11} \\
& + r_1 r_6 c_{i,12} + r_2^2 c_{i,13} + r_2 r_3 c_{i,14} + r_2 r_4 c_{i,15} + r_2 r_5 c_{i,16} \\
& + r_2 r_6 c_{i,17} + r_3^2 c_{i,18} + r_3 r_4 c_{i,19} + r_3 r_5 c_{i,20} + r_3 r_6 c_{i,21} \\
& + r_4^2 c_{i,22} + r_4 r_5 c_{i,23} + r_4 r_6 c_{i,24} + r_5^2 c_{i,25} + r_5 r_6 c_{i,26} \\
& + r_6^2 c_{i,27}
\end{aligned}
\tag{5}
$$

where $c_{i,1}...c_{i,27}$ are the calibration coefficients for an specific aerodynamic component.

Some methods of regression analysis are applying for a better data fitting of the simulations cases and thus minimise the experiments to obtain a reasonable solution. From [9], Least Squares method is suggested for aerodynamic force balances that using strain gauges in wind tunnel applications.

6.1. Weighted Least Squares Method Formulation

The least squares method provides a mathematical procedure that create a model which fit better the experimental data. Lets use N sets of aerodynamics components, each set has a response of the 27 arrangements of the six r_j. the quantities are represented now such as: $f_{i,p}$ and $r_{p,m}$ where $p = 1, ..., N$ and $m = 1, ..., 27$.

The least squares search the coefficients by minimise the sum of squared errors [8]. To minimise the function, the partial derivation is required with respect to each of the coefficients, and these partial derivatives must be zero. This procedure result in 27 equations and 27 unknowns for each f_i component.

Taking the model described in Equation (5), the least squares function described in matrix notation is

$$
f = Rc + \epsilon
\tag{6}
$$

where the vector f (size N) correspond to the observations, matrix R (size $N \times 27$) has the sensing bar force in its rows for each calibration loading, the vector c is the regression coefficients, and ϵ the random errors.

Applying the least-squares criteria that minimises the sum of squared errors, the least-squares estimator of C can be describe as

$$
C = (R^T W R)^{-1} R^T W f
\tag{7}
$$

where W is the weighting matrix, diagonal matrix of size $N \times N$.

6.2. Weighted Scheme

The formulation of the weighted matrix has many approachs concerning the references. Since W is a improvement of values precision but its computation methodology will set the complexity of the problem. The weighting matrix approach described in [10] is a current and extensive process to minimise the uncertainty of the applied loads and random errors in the measurement procedure. The construction of the weighted matrix considers two contributions to the uncertainties of the applied loads, the contributions of the sources of errors due to the application of weights in the calibration system V_W and the uncertainties in the readings of the bridges V_R, expressed as

$$
W = (V_W + D V_R D^T)^{-1}
\tag{8}
$$

where
- The matrix V_W is diagonal of size $N \times N$. Its elements are based on the uncertainties of the weights used in the loading sequence and in an estimation of the uncertainties caused by the calibration system. The second contribution, is based on the quantification of the sources of error that affect the resolution of the calibration system such as frictional forces and misalignment between cables and pulleys.
- The uncertainty of the reading values can be mitigated by repeating the the same calibration several times to build V_R that is diagonal symmetric. The diagonal elements of V_R are represented by the variances and the off diagonal elements are the covari-

ances between the readings of the bridges. It has dimensions $6N \times 6N$, and each N lines correspond to each force transducer.

• The elements of matrix D $(N \times 6N)$ correspond to the sensitivity coefficients, evaluated by taking the partial derivatives of Equation (5). In this equation, only the sensitivity coefficients whose second subscripts match, i.e. corresponds to the same loading, have values different from zero.

6.3. Goodness of Fit

The least squares method settle the hypothesis that the minimises the sum of squared errors (ssE) the optimum fitting of the data is obtain. A good measurement of goodness of fit is use chi-square, which provide a ratio between the computed difference and the variance σ^2 [11]

$$\chi^2 = \frac{ssE}{\sigma^2} = \sum_{p=1}^{N} \left\{ \frac{1}{\sigma_i^2}(f_{i,p} - \hat{f}_{i,p})^2 \right\} \qquad (9)$$

Taking into account the matrix form and the relation between quantities and the number of degrees of freedom for fitting the data point, $v = N - m$. This leads to the reduced chi-square,

$$\chi_v^2 = \frac{\chi^2}{v} = \frac{(F - \hat{F})^T W (F - \hat{F})}{N - m} \qquad (10)$$

The fitting function is a good approximation to the parent function, if χ_v^2 is approximately 1. That means the estimated variance of the fit should agree with the parent variance.

6.4. Calibration Setup and Results

The calibration is performed by applying a sequential weight load in the axes directions. In the Z direction the weights can be applied directly on top of the force balance. The X and Y directions require the use of a pulley to transfer the vertical load into a horizontal load, Figure 12.

Figure 12: Apparatus with a pulley to create a F_X.

The calibration was composed by 87 loading combinations, divided in 11 loads for each pure force and 18 loads for each composed load. The loading sequence was applied 3 times under the same conditions. A pair of weights of approximately 10N,

17N, 44N, 50N and 100N was incremented sequentially using an adequate support for the axial loads.

Concluded the third iteration of calibration procedure, the calibration coefficients for the aerodynamic force balance are obtained, some of them are shown in Table 3.

coefficient	F_X	F_Y	F_Z	M_X	M_Y	M_Z
$c_{i,1}$	-0,617896	0,090931	-1,238098	-0,088204	-0,229695	0,167224
$c_{i,2}$	-0,133195	0,043550	-1,538156	0,064625	-0,032167	0,049581
⋮	⋮	⋮	⋮	⋮	⋮	⋮
$c_{i,26}$	-0,006707	0,008181	0,008594	-0,002857	-0,002686	-0,003020
$c_{i,27}$	-0,000170	0,000569	0,004413	-0,000300	-0,000166	-0,001171

Table 3: Calibration coefficients.

The evaluation of fitting using the χ^2 and χ_v^2 can be computed with the values of $\hat{F}$ and Equation (10). The values are shown in Table 4.

Load cell	χ^2	χ_V^2
F_1	386.69	6.445
F_2	244.40	4.073
F_3	498.49	8.308
F_4	30.29	0.505
F_5	73.09	1.218
F_6	39.90	0.665

Table 4: Goodness of fit χ^2 and χ_v^2.

Some values of χ_v^2, which are not close to unit, suggest the experimental calibration procedure should be investigated. The reduced chi square of the axial forces greater than expected can be consequence of the quantification of the uncertainties. The lower number of loads, the high forces applied and the non-symmetry of the loading, compared with the other three load sets, can be the cause of the deviation.

7. Testing

The aerodynamic force balance will operate with the Técnico Aerospace Engineering Laboratory wind tunnel. The closed wind tunnel airspeed can be regulated by $v_w = 1.49 f_w - 0.25$, where v_w (m/s) stands for wind tunnel airspeed and f_w (Hz) inverter frequency. This equation comes up from the linear regression made for the points of the experimental test carried out to calibrate the wind tunnel air stream speed and the inverter frequency.

7.1. Testing Setup

The force balance should be placed in the test section of the wind tunnel, the flow is practically uniform on the entire test section. The proximity of the force balance and the nozzle can be adjusted for the necessities of the test model. The height of the force balance position can be regulated by adding structures to ensure the flange is under the lower limit of the nozzle, ensuring that instrumentation and structure do not interact with the flow.

The 5m USB cable allows the connection between the USB hub and the computer placed outside the wind tunnel. Figure 13 shows the experimental apparatus with the force balance set in the wind tunnel and with a test model.
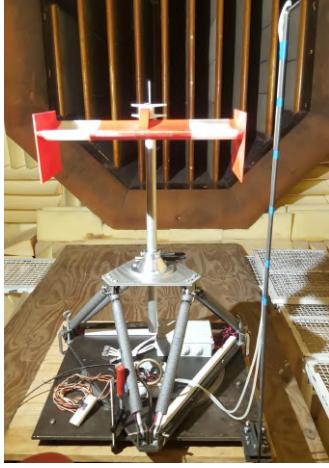

Figure 13: Experimental apparatus.

7.2. Testing Demonstration

The experimental test used a model of the rear wing of a racing car creates by the formula student team of Instituto Superior Técnico (FST).

The experimental test aimed to study the influence in drag and down force of the rear wing endplates. Flat endplates, Figure 14 (a), and curved endplates profile, Figure 14 (b), were created.
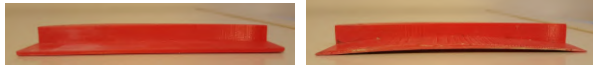

(a) Flat endplates profile.   (b) Curved endplates profile.

Figure 14: Experimental model for analysis.

The wind tunnel tests considered three different rear wing configurations, without endplates, flat and curve endplates and the quantities of study are the F_X, the F_Z and M_Y for the average velocity of the racing car in circuit, around 15m/s. Due to the use of a scale model, this velocity must be converted to conserve the aerodynamic influence by means of Reynolds number. The resulting equivalent velocity is around 37m/s. Three additional velocities were introduced in the experiment to gather more data about the response of the rear wing with the change in airspeed and the response of the force balance.
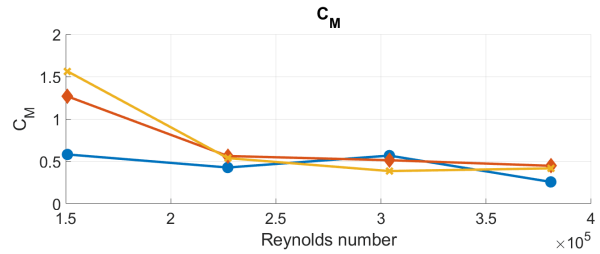
These values of force and moment were converted to the dimensionless coefficients (C_D, C_L and C_m) considering the wing dimensions and the atmospheric conditions of that day. These coefficients are presented in Figure 15, where the values of C_D and C_L obtained from CFD [12] are also presented.
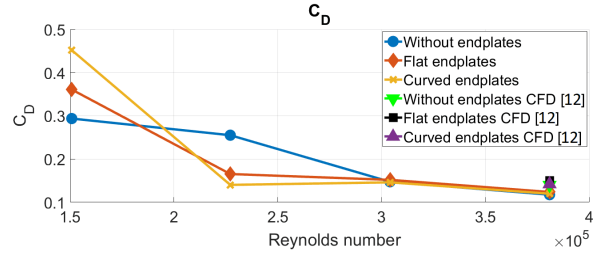
(a) Response in F_X.
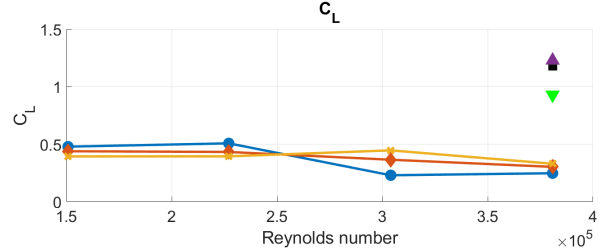
(b) Response in F_Z.

(c) Response in M_Y.

Figure 15: Results of experimental test with the three configurations.

Unfortunately, the drag contribution due to the force balance structure was not computed because the time available to use the wind tunnel facilities. However, the drag can be analysed in tendency, as well as the quantities with the same Reynolds number.

The drag coefficient tendency for the required speed (37m/s) is in agreement with the CFD analysis. The direct reduction of drag was not the main goal in the endplate analyses, in fact, the almost equal drag obtained for the flat and curved endplates is in coherency with the CFD.

The main goal, the improvement of lift using curved endplates instead of flat endplates is achieved. An increment of 4.15% of lift was obtained from the CFD, the experimental test complement with an improvement of 9%. Normally, a different between computational and experimental is expected.

From the C_L and C_D results throughout the variation of velocity, the Reynolds number has a strong influence in the performance of the endplates. Further studies should be performed to to detail its influence.

The results obtained from the two methodologies

follow the same tendency and the relation between different configurations are similar. However, the quantities obtained were different in terms of magnitude. This observation requires more tests with the force balance and analysis with CFD. Furthermore, the flow conditions and properties during the experimental test were not replicated in the CFD analyses. However, the substantial disparity highlights the need of a more comprehensive calibration.

8. Conclusions

The main goal of this work was to endow Aerospace Engineering facilities with an aerodynamic force balance capable of measuring six components. Intermediate analyses and assumptions from the most varied fields were carried out to suit the aerodynamic force balance to the desired specifications and all the tasks were overcome to achieve a proper soluction at a reasonable cost.

The adaptation of the design to fulfil the requirements demanded the finite elements analysis which produced the accurate values to support redimensioning of components. Furthermore, the experimental tests performed in the design phase validated the subsequent implementation and proved to be a good practice in works with a more practical component.

The implementation of the strain gauges was made following the specifications and taking additional care. Despite all that, the strain gauge placement always had some variation from the ideal placement. Adding the fact of the material properties and geometry possesses a deviation from the considered baseline. Therefore, the characterisation of each assembled strain gauges and sensing bar became a very favourable approach to dissipate some errors of this nature.

The experimental procedure to calibrate expose the strong dependence between a good fitting values and a good execution and employment of specific apparatus. The adopted mathematical assumption takes into account the number of inputs and the problem nature, second order is the minimum to achieve positive fitting with reasonable computation effort. The introducing of sensing bar strain gauge equation in the middle of the process was beneficial to scatter the uncertainties of the fitting coefficients.

The values obtained in the rear wing model experiment support the conclusions drawn from the CFD analysis and, this way, ensure that the new rear wing configuration will optimise the performance of racing race car when implemented in it. The influence of the velocity, and consequently the Reynolds, was an additional beneficial result from the experimental analysis.

References

[1] Jewel B. Barlow, William H. Rae, and Alan Pope. *Low-Speed Wind Tunnel Testing*. Wiley, 3rd edition, 1999. ISBN: 978-0471557746.

[2] Cameron Tropea, Alexander L. Yarin, and John F. Foss. *Springer handbook of experimental fluid mechanics*. Springer Science & Business Media, 1st edition, 2007. ISBN:978-3662491621.

[3] Jaehoon Lee. *Investigation of quality indices of in-parallel platform manipulators and development of Web-based analysis tool*. PhD thesis, University of Florida, 2000.

[4] Richard G. Budynas and J. Keith Nisbett. *Shigley's Mechanical Engineering Design*. McGraw-Hill Education, 10th edition, 2014. ISBN:9780073398204.

[5] Jr. William N. Sharpe. *Springer handbook of experimental solid mechanics*. Springer Science & Business Media, 1st edition, 2008. ISBN:978-0-387-26883-5.

[6] Manon Kok, Jeroen D. Hol, and Thomas B. Schön. Using inertial sensors for position and orientation estimation. *Foundations and Trends in Signal Processing*, 11(1-2):1–153, 2017.

[7] *National Instruments*[TM]. Getting started guide ni 9237, Accessed: Nov 2019. Online at: http://www.ni.com/pdf/manuals/374186f.pdf.

[8] Douglas C. Montgomery, Elizabeth A. Peck, and G. Geoffrey Vining. *Introduction to Linear Regression Analysis*. John Wiley & Sons, Inc., 5th edition, 2012. ISBN: 978-0-470-54281-1.

[9] AIAA. *Recommended Practice: Calibration and Use of Internal Strain-Gage Balances with Application to Wind Tunnel Testing*. American Institute of Aeronautics and Astronautics, 1st edition, 2003. DOI: 10.2514/4.476464.001.

[10] M.L.C.C. Reis, R.M. Castro, and O.A.F. Mello. Calibration uncertainty estimation of a strain-gage external balance. *Measurement*, 46(1):24–33, 2013.

[11] Philip R. Bevington and D. Keith Robinson. *Introduction to Linear Regression Analysis*. McGraw-Hill, 3rd edition, 2003. ISBN: 978-0072472271.

[12] Tiago Pereira Rocha. Numerical and experimental study of wing tip endplates of a formula student car. Master's thesis, Instituto Superior Técnico, October 2020.